1

Comparing the potential of multispectral and hyperspectral data for monitoring oil spill impact

Shruti Khanna
Center for Spatial Technologies and Remote Sensing
Department of Land Air and Water Resources
University of California
One Shields Avenue,
Davis, CA, USA
Email: shrkhanna@ucdavis.edu

Maria J. Santos
Department of Innovation, Environmental and Energy Sciences
Utrecht University
Utrecht, Netherlands

Department of Geography
University of Zürich
Zürich, Switzerland

Susan L. Ustin
Center for Spatial Technologies and Remote Sensing
Department of Land Air and Water Resources
University of California
Davis, CA, USA

Kristen Shapiro
Center for Spatial Technologies and Remote Sensing
Department of Land Air and Water Resources
University of California
Davis, CA, USA

Paul J. Haverkamp
Center for Spatial Technologies and Remote Sensing
Department of Land Air and Water Resources
University of California
Davis, CA, USA

Mui Lay
Center for Spatial Technologies and Remote Sensing
Department of Land Air and Water Resources
University of California
Davis, CA, USA

Keywords: vegetation indices, LANDSAT, WorldView-2, RapidEye, AVIRIS

Abstract

Oil spills from offshore drilling and coastal refineries often cause degradation of coastal wetlands that can take a long time to recover. Early oil detection may prevent losses and speed up recovery if monitoring of the initial oil extent, oil impact, and recovery are in place. Satellite imagery data can provide a cost-effective alternative to expensive airborne imagery or labor intensive field campaigns for monitoring effects of oil spills on wetlands. However, these satellite data may be restricted in their ability to detect and map ecosystem recovery post-spill given their spectral measurement properties and temporal frequency. In this study, we assessed whether spatial and spectral resolution, and other sensor characteristics influence the ability to detect and map vegetation stress and die-off due to oil. We compared how well three satellite multispectral sensors: WorldView2, RapidEye and Landsat EMT+, match the ability of the airborne hyperspectral AVIRIS sensor to map oil-induced vegetation stress, recovery, and die-off after the DeepWater Horizon oil spill in the Gulf of Mexico in 2010.

We found that finer spatial resolution (3.5m) provided better delineation of the oil-impacted wetlands and better detection of vegetation stress along oiled shorelines in saltmarsh wetland ecosystems. As spatial resolution become coarser (3.5m to 30m) the ability to accurately detect and map stressed vegetation decreased. Spectral resolution did improve the detection and mapping of oil-impacted wetlands but less strongly than spatial resolution, suggesting that broad-band data may be sufficient to detect and map oil-impacted wetlands. AVIRIS narrow-band data performs better detecting vegetation stress, followed by WorldView2, RapidEye and then Landsat 15m (pan sharpened) data. Higher quality sensor optics and higher signal-to-noise ratio (SNR) may also improve detection and mapping of oil-impacted wetlands; we found that resampled coarser resolution AVIRIS data with higher SNR performed better than either of the three satellite sensors. The ability to acquire imagery during certain times (midday, low tide, etc.) or a certain date is also important in these tidal wetlands; WorldView2 imagery captured at high-tide detected a narrower band of shoreline affected by oil likely because some of the impacted wetland was below the tideline. These results suggest that while multispectral data may be sufficient for detecting the extent of oil-impacted wetlands, high spectral and spatial resolution, high-quality sensor characteristics, and the ability to control time of image acquisition may improve assessment and monitoring of vegetation stress and recovery post oil spills.

1. Introduction

Coastal wetlands are important but vulnerable ecosystems that provide valuable ecosystem services such as protection from storms and storm surges, support for fisheries and seafood industries, nursery sites for juvenile fish, carbon storage, nutrient cycling, waterfowl habitat and other key services [1-8]. Coastal wetlands are also subject to relatively frequent disturbances such as hurricanes and other storms, changes in sea level, and contamination from runoff, tidal inputs, and oil spills, all of which cause vegetation stress and wetland degradation and die-off [9-13] which can cause lasting damage for years to decades [13-16]. Since 1973, both the volume and number of oil spill incidents has declined in the United States [17]. However, large oil spill events still cause disproportionate impacts in the wetlands where they occur. The DeepWater Horizon (DWH) Oil Spill in the Gulf of Mexico in 2010 was the biggest oil spill in the US history and the second-largest in the world [18]. The DWH spill occurred in deep oceanic pipelines, which were difficult to contain. In total, 206 million gallons of oil were released over 85 days from 20 April to 19 July, which contaminated 572 miles of gulf shoreline [18]. The effects of the DWH oil spill on the Gulf of Mexico wetlands are likely still ongoing, as demonstrated by several recent studies [16,19-24].

Oil is highly detrimental to plant health, both directly and indirectly. Oil affects plant metabolism directly as coating the leaves prevents gas exchange between the leaves and the atmosphere, significantly increasing leaf and plant mortality [25-29]. Oil also affects plants indirectly when present in the soil by reducing oxygen exchange between the atmosphere and soil, affecting the microbial community and nutrient cycling [15,25,26,30]. At the ecosystem level, post-oil spill senescent and dead plant material slowly erodes resulting in a transition from wetland to bare soil or water [25]. The recovery from oil effects can take months to several years [13,15,31],

97   especially since different wetland communities differ in their susceptibility to oil impacts

98   [14,32,33].

99   As plants become increasingly stressed, they lose pigments, water, and ultimately leaves, all of

100   which can be measured through changes in their reflectance [34-38]. Plant stress affects plant

101   reflectance in regions of the electromagnetic spectrum related to plant pigment concentration

102   [35-37,39,40], water content [41-43], and leaf area or canopy density [44]. Most multispectral

103   satellite sensors have at least four fundamental bands: Blue, Green, Red, and Near InfraRed

104   (NIR) [45]. Vegetation indices based on these bands are effective in tracking both pigment and

105   leaf area [46,47]. The Shortwave InfraRed (SWIR) band is available on some freely available

106   multispectral sensors like Landsat or the European Space Agency's Sentinel-2 "Landsat-like"

107   satellites and is used to measure plant water content [43]. Vegetation indices calculated from

108   imaging spectrometers can track all of these changes as demonstrated by Khanna et al. [20] after

109   the DWH oil spill. Change in land cover due to loss of wetland vegetation can be tracked through

110   "angle indices", which are relatively insensitive to the confounding influence of soil moisture

111   [44,48]. Thus, imaging spectrometer data is useful in mapping and monitoring oil spill impacts

112   on wetland extent and oil induced vegetation stress [49-52].

113   While many studies have mapped oil extent with multispectral imagery [30,53,54], hyperspectral

114   imagery [55,56], and RADAR [57-59], few have assessed the post-oil spill stress on wetland

115   vegetation, and then, most have used imaging spectrometer data [20,49,60-62]. The objective of

116   this study is to explore the potential for using easily available multispectral sensor data to detect

117   and map vegetation stress and die-off due to oil contamination. We sought to determine whether

118   oil-induced plant stress can be detected and monitored using multispectral satellite imagery with

119   fine (WorldView-2 and RapidEye; 2m and 5m) and moderate spatial resolutions (Landsat

120   ETM+; pan sharpened 15m or 30m). We contrast multispectral sensors with airborne AVIRIS

121   imagery in their abilities to detect vegetation stress in oiled versus oil-free shores. Each sensor

122   has different characteristics regarding spectral, spatial, and radiometric resolution, and sensor

123   engineering, all of which might influence the potential of the sensor data to monitor oil spill

124   impacts.

2. Data and methods

126   *2.1 Study area*

127   Barataria Bay is located approximately 160 km from the DWH oil spill site in an interlobe basin

128   between the current Bird's Foot delta and the abandoned Lafourche delta lobes [63]. The

129   dominant plant species in the low intertidal saltmarshes is *Spartina alterniflora* (saltmarsh

130   cordgrass) and *Juncus roemerianus* (needlegrass rush), with subdominants *Spartina patens* (salt

131   meadow cordgrass), *Distichlis spicata* (saltgrass) and *Batis maritima* (saltwort) more common in

132   the higher marsh [64]. Since the DWH oil spill occurred offshore, the oil came in with the tides

133   and primarily contaminated the seaward edges of the wetlands (Figure 1). Several studies

134   mapped the oil spill extent in the ocean [65-68] and the wetlands [69], and its detrimental effects

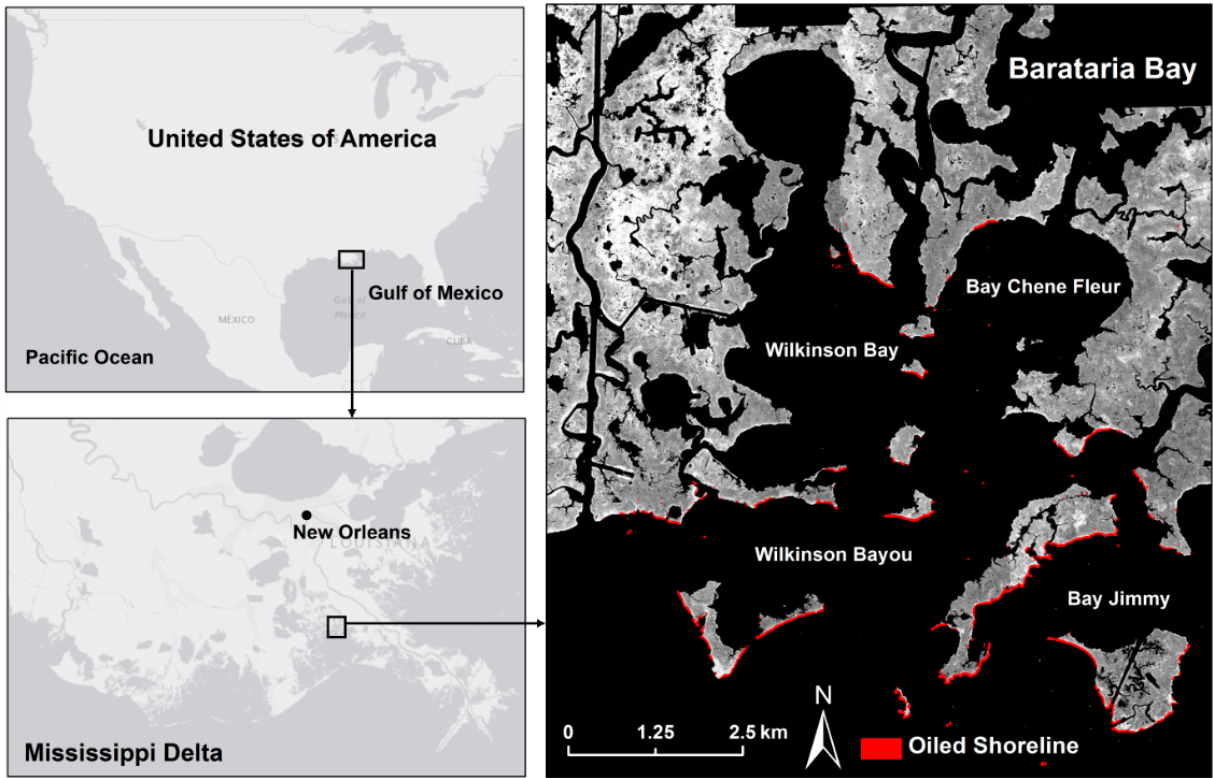135   on the wetland vegetation [20,22].

136

6

Figure 1: AVIRIS gray scale image of Barataria Bay and its location in the Mississippi Delta. Oil mapped using AVIRIS 2010 imagery is overlaid in red.

2.2 Image data and preprocessing

AVIRIS data was acquired over Barataria Bay and used to map the presence of oil along the wetland shoreline and to detect plant stress due to oil contamination on vegetation [20]. Four flight-lines covering an area of 175 km^2 (Table 1) were georeferenced by NASA Jet Propulsion Laboratory using information derived from inertial navigation data and GPS. Unfortunately, images georeferenced based on this information often suffer from residual misalignment by a few pixels or more, and this misalignment translated into displacements of the order of dozens of meters, whereas oil penetration and impact was unequal near the shore exhibiting sharp gradients on the scale of just a few meters [20,70]. Hence the 2010 images were further georectified to 1m National Agricultural Imagery Program (NAIP) color infrared images collected in 2010. Images

151   were also atmospherically calibrated using the Atmospheric CORrection Now algorithm

152   (ACORN) 6, mode 1.5 (ImSpec LLC, Seattle) to apparent surface reflectance.

153   **Table 1:** Characteristics of the four sensors and date of image acquisition for data analyzed in this study.

	AVIRIS	WorldView2	Rapid Eye	Landsat ETM+
Bandwidth	10-15nm	40-180nm	40-90nm	60-260nm
Spatial resolution	3.5m	2m	5m	15m, 30m
Radiometric resolution	16-bit	11-bit	16-bit	8-bit
Time of acquisition	Sep 19, 2010	Sep 8, 2010	Oct 8, 2010	Sep 13, 2010
Signal-to-noise ratio	800-1200 [71]	250-500 [72]	90-140 [73,74]	20-55 [71,75]
Cloud cover	0%	30%	0%	0%

154

155   Seventeen multispectral WorldView2 images (Table 1) covering the same area as AVIRIS were

156   atmospherically calibrated to apparent surface reflectance and mosaicked. Two RapidEye images

157   were also calibrated to apparent surface reflectance and mosaicked. Finally, one Landsat ETM+

158   image was calibrated to apparent surface reflectance using ACORN 6, mode 5. Since both

159   WorldView2 and RapidEye data were acquired off-nadir, we could not use ACORN for

160   atmospheric correction. Hence we used Atmospheric Correction and Haze Reduction (ATCOR)

161   [76] which allows input of non-nadir view angles. Moreover, it performs at least as well as

162   ACORN and the results of the two calibration techniques are comparable, especially over a flat

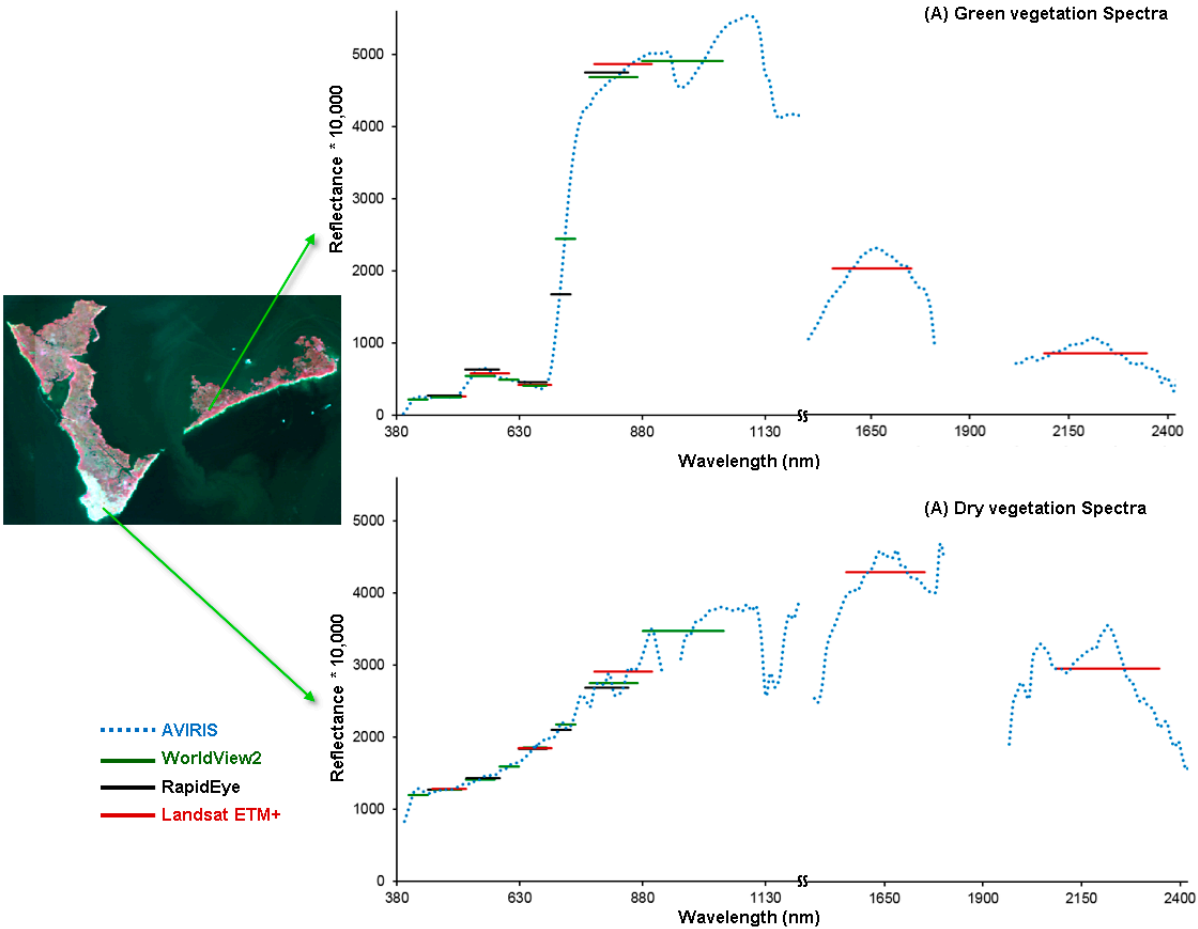163   terrain such as Barataria Bay [77].

Figure 2: Barataria Bay gray scale image subset for all four sensors and a close view of a smaller region to highlight differences in image quality and spatial resolution (a) AVIRIS 3.5m imagery, (b) WorldView2 2m imagery, (c) RapidEye 5m imagery, and (d) Landsat ETM+ 30m imagery.

All images from the three multispectral sensors were subset to the spatial extent of the oil-affected section of the study area (Figure 2, 86 km^2). Both WorldView2 and RapidEye image mosaics were further geographically co-registered to the AVIRIS 2010 imagery using an automated image registration technique [78,79] to enable comparisons between the different sensors. The advantage of this technique is that areas of spurious change can be excluded, e.g. clouds in one image or shoreline changes with varying tidal stage. We were able to exclude these

175   areas from calculations of displacement between images, hence the tidal stages of different

176   images did not affect the accuracy of co-registration.

177   We mapped oil on exposed soil surfaces and dry vegetation, and water and land pixels in the

178   AVIRIS 2010 images using a binary decision tree following methods in Khanna et al. [80].

179   Inputs to the decision tree included vegetation and angle indices and continuum removals [81]

180   over two well-known oil absorption features centered at 2100nm and 2300nm [69]. Binary

181   classes, land and water, were mapped in addition to oiled pixels.

182   The United States Geological Survey (USGS) conducted field data surveys in Barataria Bay on

183   July 10, 2010 and again on August 12-13, 2010 [82]. At each 2 x 2 m survey point, they

184   collected information on the vegetation species composition, canopy condition, presence of oil,

185   and penetration of oil into the marsh. We randomly chose half the points for training the

186   classifier to recognize oiled pixels and the other half to test the accuracy of detecting oiled pixels

187   using Kappa statistics, and overall classification accuracy [83,84]. The results of this

188   classification were first presented in Khanna et al. [20] showing that the oiled pixels were

189   classified with an overall accuracy of 95% and a Kappa of 0.88.

190   ***2.3. Methods***

191   *2.3.1 AVIRIS hyperspectral data*

192   To compare the effect of sensor spectral and spatial resolution on detecting plant stress, we

193   spectrally resampled AVIRIS hyperspectral data to simulate the WorldView2, RapidEye, and

194   Landsat ETM+ sensors using pre-defined filter functions available in ENVI 4.8 (ITT Visual

195   Information Solutions). Next, we resampled the simulated images to the spatial resolution of

196   these sensors, 5m for RapidEye and 30m for Landsat ETM+, using pixel aggregate and bilinear

197   convolution methods when appropriate in ENVI 4.8. We pan-sharpened the 30m simulated

198   Landsat imagery to 15m spatial resolution using the Gram-Schmidt pan-sharpening method

199   available in ENVI 4.8 [85]. Since the spatial resolution of the original AVIRIS imagery was

200   3.5m and it is technically impossible to get better resolution imagery by resampling a coarser

201   resolution image, we did not recreate the 2m WorldView2 resolution for the simulated

202   WorldView2 imagery. We will refer to these resampled image data in our study as $AVIRIS_{WV2}$,

203   $AVIRIS_{RE}$, $AVIRIS_{LS-30m}$ and $AVIRIS_{LS-15m}$.

204   *2.3.2. Multispectral sensor data*

205   In addition to varying spatial and spectral resolution, sensors also differ in other characteristics,

206   such as lens distortion and signal-to-noise parameters, which can affect their performance in

207   measuring the phenomena of interest [71,73]. Hence, the next step in our study was to compare

208   the ability to detect oil-induced vegetation stress from images acquired by WorldView2,

209   RapidEye, and Landsat 7 ETM+ sensors to that of the AVIRIS image using dates as close to the

210   AVIRIS image date as was available. The WorldView2 and Landsat images were acquired

211   within a week of the AVIRIS image acquisition date while the RapidEye image was within a

212   month of that date (Table 1). The Landsat ETM+ image was further pan-sharpened to 15m pixel

213   resolution using the Gram-Schmidt pan-sharpening method available in ENVI 4.8 [85]. Figure 3

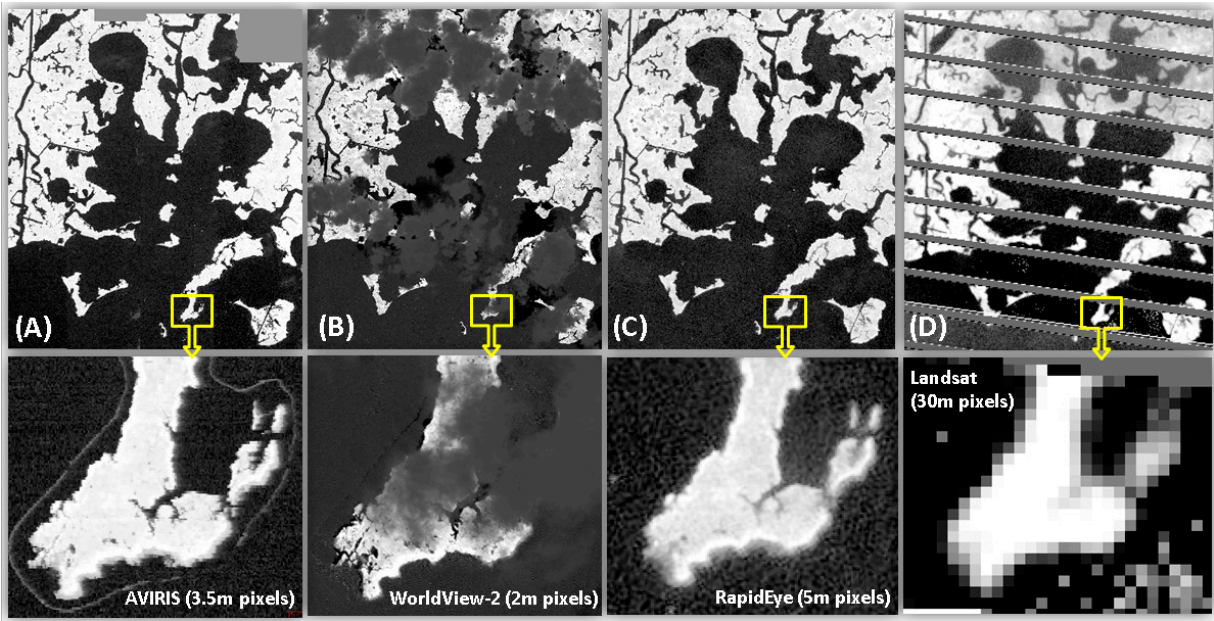214   illustrates the different spectral resolutions of the four sensors.

Figure 3: An example of (a) green vegetation and (b) non-photosynthetic vegetation (NPV) pixel spectra from AVIRIS, WorldView2, RapidEye, and Landsat ETM+ showing the range and spectral resolution of the sensors.

2.3.3. Selection of oiled and oil-free areas

We following a consistent procedure to assign shorelines as either oiled or oil-free and extract pixels along those shorelines for analysis. First, based on the classification of the 2010 AVIRIS image dataset, we used the boundary of the land and water classes to produce a vector layer of the shoreline. Next, sections of the shore with oiled pixels adjacent to them were considered as oiled shoreline. Sections of shore next to oil-free pixels were considered as oil-free shoreline. Only oil-free shoreline within 140m of an oiled shoreline was used for comparison to ensure that the sites used were as similar to each other as possible, except in the degree of oiling. Finally, we extracted all pixels within 60m perpendicular to and inland from shore of the selected shorelines compare vegetation stress between oiled and oil-free shorelines.

We subdivided the extracted pixels from the images into zones parallel to the shoreline. A zone is defined as the line of pixels parallel to the shore where each pixel within that zone is away

230   from the shore by the same distance measured in pixel width. For example, zone 1 corresponds

231   to the first pixel adjacent to the shore, zone 2 corresponds to two pixels from the shore, and so

232   on. The width of the zones was determined by the image pixel size. We chose to compare

233   corresponding zones parallel to the shoreline because wetland species distributions, abundance

234   and changes in composition follow elevation gradients [86]. In the gulf wetlands the remote

235   sensing data reveals an inherent spatial pattern irrespective of other impacts: vegetation is

236   moderately dense in the intertidal zone followed by a band of more dense and green vegetation

237   that occurs just beyond the intertidal zone, and then slightly lower density in the inner marsh

238   [20]. Thus by comparing within zones, we minimized the confounding effects of these inherent

239   spatial patterns in wetland vegetation communities.

240   *2.3.4 Detection of vegetation stress*

241   We calculated four vegetation indices based on the Green, Red, NIR and SWIR bands:

242   Normalized Difference Vegetation Index (NDVI), Normalized Difference Infrared Index (NDII),

243   Angle at Near InfraRed (ANIR) and Angle at Red (ARed; Table 2). The bandwidth and

244   wavelength centers of the bands in these general electromagnetic regions were dependent on the

245   sensor specifications, e.g. while AVIRIS had narrow 10-15nm bands, the three multi-spectral

246   sensors had much broader bands from 40nm to 260nm (Table 1). For WorldView2, RapidEye,

247   AVIRIS$_{WV2}$ and AVIRIS$_{RE}$, we only calculated NDVI and ARed since both ANIR and NDII

248   require a SWIR band, which WorldView2 and RapidEye lack. For the Landsat and AVIRIS$_{LS}$

249   images, we calculated all four indices. We did not radiometrically calibrate the different sensor

250   images because our comparisons are between pixels of the same image rather than between

251   sensors. The purpose is to compare the ability of sensors to differentiate healthy vegetation from

252   stressed vegetation within the same image and this can be done effectively by using a statistical

253 approach that is independent of the range and magnitude of index values and then comparing the

254 statistic across sensors.

255 **Table 2:** Vegetation indices used to test for the effects of oil contamination on vegetation stress, and the sensors
256 they were calculated for. R_G, R_R, R_{NIR} and R_{SWIR} are the reflectance values in the Green (G), Red (R), Near InfraRed
257 (NIR) and ShortWave InfraRed (SWIR) bands respectively and λ_G (550-570nm), λ_R (650nm), λ_{NIR} (805-840nm) and
258 λ_{SWIR} (1650nm) are the wavelength values at the band centers.

Inputs	Formula	Relevance	References	Index calculated using Sensors
Normalized Difference Vegetation Index (NDVI)	$\dfrac{R_{NIR} - R_R}{R_{NIR} + R_R}$	Index of green plant cover and LAI	[46,47]	AVIRIS
Normalized Difference Infrared Index (NDII)	$\dfrac{R_{NIR} - R_{SWIR}}{R_{NIR} + R_{SWIR}}$	Sensitive to plant water content	[43,87]	AVIRIS, Landsat
Angle at NIR (ANIR) (rad)	Angle between (R_R, λ_R), (R_{NIR}, λ_{NIR}), and (R_{SWIR}, λ_{SWIR})	Angle index sensitive to change in land cover type	[44,88]	AVIRIS
Angle at Red (ARed) (rad)	Angle between (R_G, λ_G), (R_R, λ_R), and (R_{NIR}, λ_{NIR})	Angle index sensitive to plant pigments and land cover type	[20,88]	AVIRIS, WorldView2, RapidEye, Landsat

259

260 Effect size is a statistic that measures the degree of overlap between the frequency distributions

261 of two samples; if the frequency distributions overlap it suggests the two samples come from the

262 same population i.e. are not differentiable, while when there is little or no overlap, it suggests

263 that the two samples are not from the same population. The greater the overlap in the frequency

264 distributions, the lower the effect size and vice versa. Effect size is a good metric because it is

265 independent of sample size and the range of index values. To determine differences in plant

266 stress along oiled vs. oil-free shorelines, we first tested whether average index values were

267 different in pixels alongside oiled and oil-free shorelines by using a t-test [89]. To assess the

268   magnitude of the differences in index values, we calculated the effect size, Cohen's d [90].

269   Cohen's d is a standardized metric of the difference between two means as it divides the

270   population mean by the pooled standard deviation, allowing for comparisons across many

271   variables and sensors [90,91]. A Cohen's d value of 0.8 indicates a strong effect, i.e. little

272   overlap between the two frequency distributions suggesting a strong ability to differentiate

273   between the two samples, a value of 0.5 indicates a moderate effect, while a value lower than 0.2

274   indicates a weak effect [90].

275   ## 3   Results

276   ### *3.1 AVIRIS hyperspectral data*

277   The first 14m (4 pixels) along the oiled shore in the AVIRIS hyperspectral imagery have

278   significantly more stressed vegetation than the corresponding oil-free zone. All indices had

279   significantly lower values (ANIR has the reverse order with higher values indicating lower

280   stress) along the oiled shoreline relative to the oil-free shore line, (Table 3). Despite all zones

281   showing significant differences in index values, the effect size decreased as we moved inland

282   from the shore indicating that oil-induced vegetation stress decreased away from the shore

283   (Table 3).

284   While all four indices detect plant stress effectively, ARed (average Cohen's d = 0.81) and NDII

285   (average Cohen's d = 0.80) exhibited the strongest effect sizes, thus performing better at

286   differentiating vegetation stress due to oil contamination. In the first zone, where the oil impact

287   was expected to be maximum, average value of ARed dropped from 5.12 along oil-free shores to

288   4.11 along oiled shorelines, while average value of NDII dropped from 0.51 to 0.33 (Table 3).

289   Hence, we selected ARed for a comparison of all four sensors and NDII for an additional

290   comparison of Landsat ETM+ and AVIRIS.

291   **Table 3:** Student t-test comparison results for four indices calculated with AVIRIS data. Value of Cohen's d
292   indicates effect size.

Index	Zone	N		Mean		Std. Dev.		student t-statistic	p-value	Cohen's d
		oiled	oil-free	Oiled	oil-free	oiled	oil-free			
NDVI	1	5539	3156	0.474	0.583	0.223	0.227	-21.560	**0.000**	0.483
	2	5220	3118	0.618	0.676	0.178	0.192	-13.614	**0.000**	0.314
	3	3941	2440	0.683	0.711	0.159	0.153	-6.933	**0.000**	0.177
ARed	1	5539	3156	4.113	5.118	0.796	0.760	-58.320	**0.000**	1.284
	2	5220	3118	4.596	5.287	0.944	0.752	-36.862	**0.000**	0.789
	3	3941	2440	5.122	5.397	0.834	0.665	-14.585	**0.000**	0.357
	4	3841	2533	5.399	5.449	0.670	0.593	-3.088	**0.002**	0.077
NDII	1	5539	3156	0.333	0.510	0.172	0.155	-49.431	**0.000**	1.072
	2	5220	3118	0.395	0.531	0.172	0.132	-40.495	**0.000**	0.858
	3	3941	2440	0.484	0.548	0.151	0.121	-18.691	**0.000**	0.457
	4	3841	2533	0.539	0.561	0.125	0.113	-7.118	**0.000**	0.179
ANIR	1	5539	3156	1.531	0.775	0.849	0.708	44.471	**0.000**	0.944
	2	5220	3118	0.940	0.503	0.802	0.554	29.361	**0.000**	0.608
	3	3941	2440	0.584	0.424	0.601	0.425	12.500	**0.000**	0.298
	4	3841	2533	0.461	0.422	0.484	0.411	3.376	**0.001**	0.084

293

294   *3.1.1 Spectral resolution*

295   Comparing the ability to detect oil-induced stress in vegetation using AVIRIS$_{WV2}$ vs. AVIRIS

296   data shows the effect of spectral resolution on oil impact detection. We found that effect size for

297   ARed decreased about 12% from AVIRIS narrow-band imagery (average for zones 1-3, Cohen's

298   d = 0.81) to AVIRIS$_{WV2}$ broad-band imagery (average for zones 1-3, Cohen's d = 0.71) (Table

299   4). In the fourth zone from the shore, ARed values between oiled and oil-free shorelines were no

300   longer significantly different using AVIRIS$_{WV2}$ data while they were still significant using

301   AVIRIS data (Table 4). Thus, the reduced spectral resolution of the AVIRIS$_{WV2}$ resulted in a

302   lower ability to discriminate vegetation stress in the most oiled zones, and a lack of

303   differentiation potential in the zone, 14m inland from shoreline (Table 4).

304   **Table 4:** Student t-test comparison results for ARed in radians calculated from AVIRIS narrow-band image and
305   AVIRIS imagery spectrally and spatially resampling to WorldView2 (AVIRIS$_{WV2}$), RapidEye (AVIRIS$_{RE}$), and
306   Landsat (AVIRIS$_{LS}$) 15m and 30m. Value of Cohen's d indicates effect size.

Sensor	Zone	N		Means		Std. Dev.		Student t-Statistic	p-value	Cohen's d
		oiled	oil-free	Oiled	oil-free	oiled	oil-free			
AVIRIS 3.5m	1	5539	3156	4.113	5.118	0.796	0.760	-58.320	**0.000**	1.284
	2	5220	3118	4.596	5.287	0.944	0.752	-36.862	**0.000**	0.789
	3	3941	2440	5.122	5.397	0.834	0.665	-14.585	**0.000**	0.357
	4	3841	2533	5.399	5.449	0.670	0.593	-3.088	**0.002**	0.077
AVIRIS$_{WV2}$ 3.5m	1	5539	3156	3.861	4.620	0.657	0.712	-49.130	**0.000**	1.120
	2	5220	3118	4.238	4.787	0.805	0.760	-31.257	**0.000**	0.697
	3	3941	2440	4.681	4.927	0.792	0.714	-12.853	**0.000**	0.323
AVIRIS$_{RE}$ 5m	1	3965	2271	0.965	1.696	0.724	0.660	-40.632	**0.000**	1.043
	2	3785	2222	1.538	1.902	0.805	0.673	-18.816	**0.000**	0.480
	3	2759	1887	1.949	1.989	0.684	0.634	-2.043	**0.041**	0.060
AVIRIS$_{LS}$ 15m	1	1318	852	4.557	4.953	0.776	0.631	-13.040	**0.000**	0.549
AVIRIS$_{LS}$ 30m	1	749	405	4.921	5.071	0.625	0.442	-4.723	**0.000**	0.264

307

308   *3.1.2 Spatial resolution*

309   AVIRIS, AVIRIS$_{RE}$, AVIRIS$_{LS-15m}$ and AVIRIS$_{LS-30m}$ represent progressively coarser spatial

310   resolutions from 3.5m to 5m to 15m to 30m pixels. Comparing the performance of the four

311   image datasets showed that loss of spatial resolution resulted in especially low effect sizes, i.e.,

312   decreased ability to detect differences in vegetation index values. A comparison of the first zone

313   next to the shore shows effect sizes dropped one order of magnitude, from 1.12 to 0.19, as spatial

314 resolution became coarser from 3.5m AVIRIS$_{WV2}$ to 5m AVIRIS$_{RE}$ to 15m AVIRIS$_{LS}$ to 30m

315 AVIRIS$_{LS}$ (Figure 4; Table 4). For example, the effect size for AVIRIS$_{LS}$ dropped by half, from

316 0.55 in the 15m pixel image to 0.26 in the 30m pixel image, indicating that the area of overlap

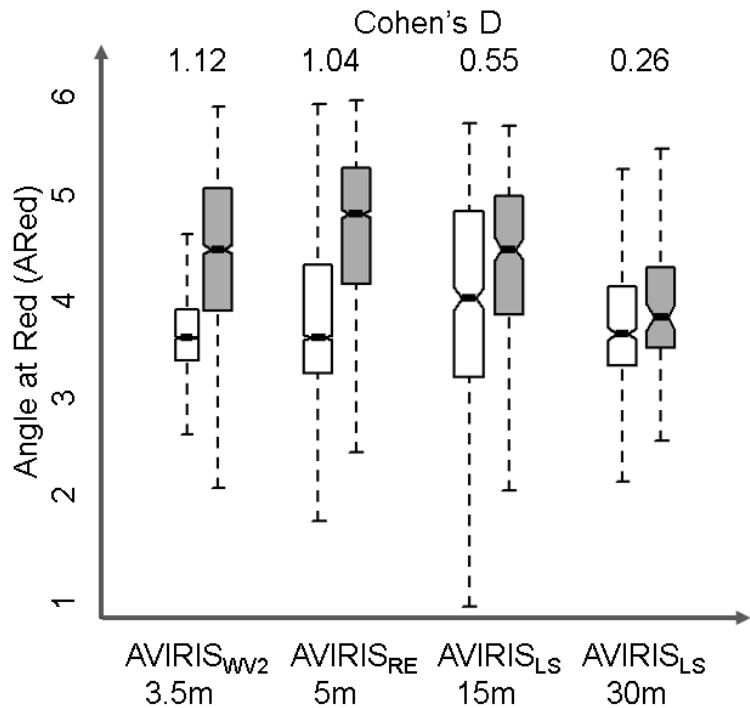317 between the oiled and oil-free index frequency distributions increased considerably.

318

Figure 4. Boxplots of the Angle at Red index in the first pixel zone along oiled (white) vs. oil-free (gray) shoreline

320 using AVIRIS imagery resampled to WorldView2, Landsat ETM+ 15m and Landsat ETM+ 30m. Notches on the

321 boxplots indicate the 95% confidence interval. Cohen's d values are shown for reference at the top.

322

323 While all four spatial resolutions were sufficient to detect significant vegetation stress in the

324 pixels located largely within the 14m zones next to the oiled shoreline, the sensitivity of that

325 detection reduced quickly with increasing pixel size. The zone of oil impact became less defined
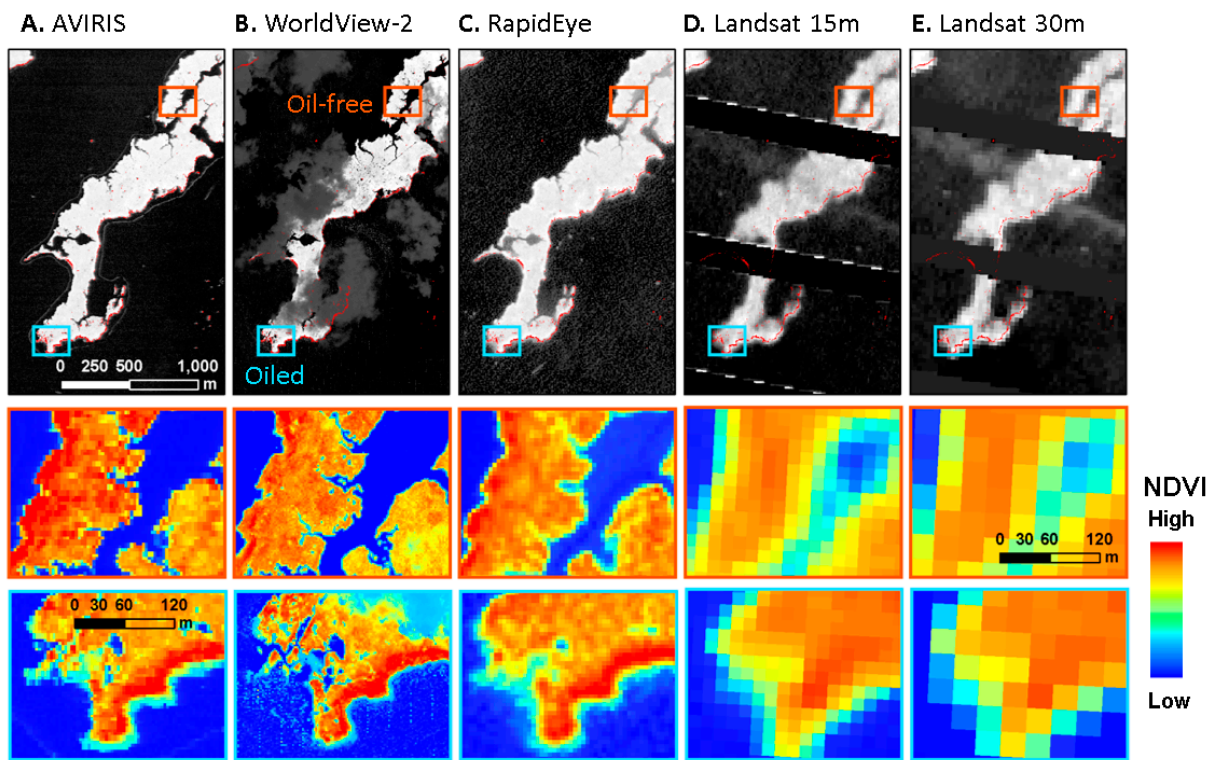
326 as zones became more mixed (Figure 5).

Figure 5. A subset of Barataria Bay shown in gray scale (*a*) AVIRIS, (*b*) WorldView-2, (*c*) RapidEye, (*d*) Landsat ETM+ pan sharpened 15m, (*e*) Landsat ETM+ 30m with oiled pixels overlaid in red. NDVI color map of an oiled and an oil-free area is detailed in the second and third rows from the top. Note the lack of spatial definition of the affected area as spatial resolution deteriorates.

3.2 Multispectral data

All three multispectral sensors, WorldView2, RapidEye and Landsat ETM+, performed worse

than the AVIRIS imagery resampled to the spatial and spectral resolution of these sensors (Table

5). Using original WorldView2 imagery, we were able to detect significant differences in index

values along oiled vs. oil-free shorelines in zones up to 10m inland (5 pixels; Table 5), which is

similar to the 10.5m distance over which significant differences were observed for $AVIRIS_{WV2}$.

However, the effect sizes for WorldView2 data were lower than those for $AVIRIS_{WV2}$ data

indicating weaker differentiation in vegetation index values. The RapidEye imagery could only

341   detect impact 5m inland (1 pixel), while AVIRIS$_{RE}$ detected oil impact up to 15m (3 pixels).

342   Again, the RapidEye effect size was less than half that of AVIRIS$_{RE}$ for the corresponding zone

343   (Figure 6, Table 5). Similarly, for Landsat, effect sizes dropped to half of those using the

344   resampled AVIRIS$_{LS-15m}$ imagery (Figure 7).

345   **Table 5.** Student t-test comparison results for ARed in radians calculated from AVIRIS imagery spectrally and
346   spatially resampled to WorldView2 (AVIRIS$_{WV2}$), RapidEye (AVIRIS$_{RE}$), Landsat (AVIRIS$_{LS}$) 15m and 30m
347   compared to the actual sensor imagery. Value of Cohen's d indicates effect size.

| Sensor	Zone	N		Means		Std. Dev.		Student t-Statistic	p-value	Cohen's d
		Oiled	oil-free	oiled	oil-free	oiled	oil-free			
AVIRIS$_{WV2}$	1	5539	3156	3.861	4.620	0.657	0.712	-49.130	**0.000**	1.120
3.5 m	2	5220	3118	4.238	4.787	0.805	0.760	-31.257	**0.000**	0.697
	3	3941	2440	4.681	4.927	0.792	0.714	-12.853	**0.000**	0.323
WV2 2m	1	5111	2223	3.553	3.721	0.594	0.606	-11.017	**0.000**	0.282
	2	6506	3067	3.577	3.938	0.462	0.531	-32.310	**0.000**	0.744
	3	6449	3202	3.794	4.013	0.546	0.549	-18.549	**0.000**	0.402
	4	4992	2576	3.986	4.093	0.575	0.591	-7.519	**0.000**	0.184
	5	4839	2588	4.114	4.161	0.544	0.557	-3.493	**0.000**	0.086
AVIRIS$_{RE}$ 5m	1	3965	2271	0.965	1.696	0.724	0.660	-40.632	**0.000**	1.043
	2	3785	2222	1.538	1.902	0.805	0.673	-18.816	**0.000**	0.480
	3	2759	1887	1.949	1.989	0.684	0.634	-2.043	**0.041**	0.060
RE 5m	1	14979	10495	4.238	4.456	0.496	0.449	-36.615	**0.000**	0.458
AVIRIS$_{LS}$ 15m	1	1318	852	4.557	4.953	0.776	0.631	-13.040	**0.000**	0.549
Landsat 15m	1	596	392	4.177	4.281	0.484	0.477	-3.330	**0.001**	0.216
AVIRIS$_{LS}$ 30m	1	749	405	4.921	5.071	0.625	0.442	-4.723	**0.000**	0.264
Landsat 30m	1	467	98	3.725	3.885	0.685	0.564	-2.453	**0.015**	0.240
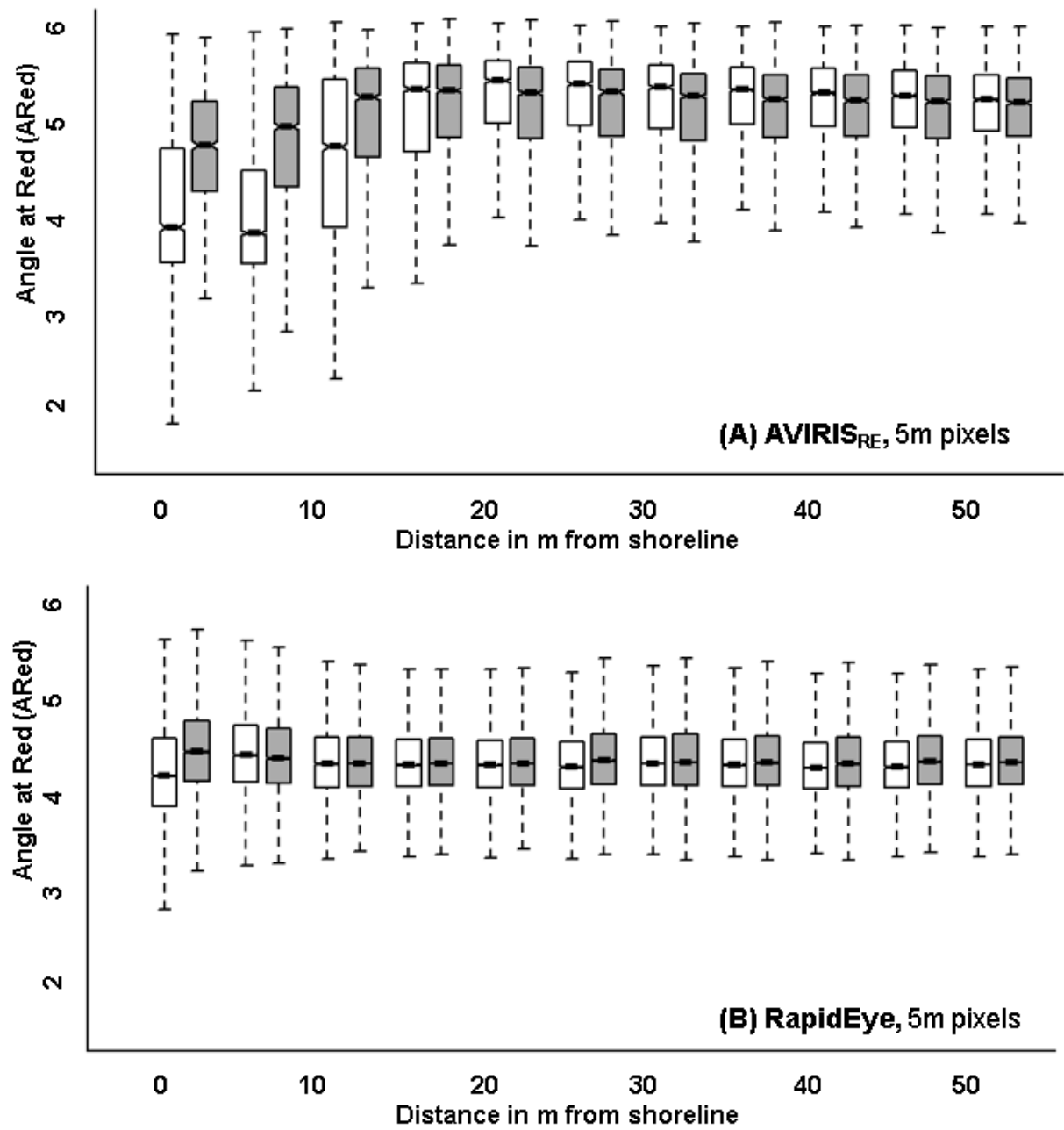
348

349

Figure 6. Angle at Red vs. distance from shoreline in meters for (*a*) AVIRIS resampled to RapidEye and (*b*) actual
RapidEye imagery. Distribution of the index along the oiled shoreline is in white and along oil-free shoreline, in
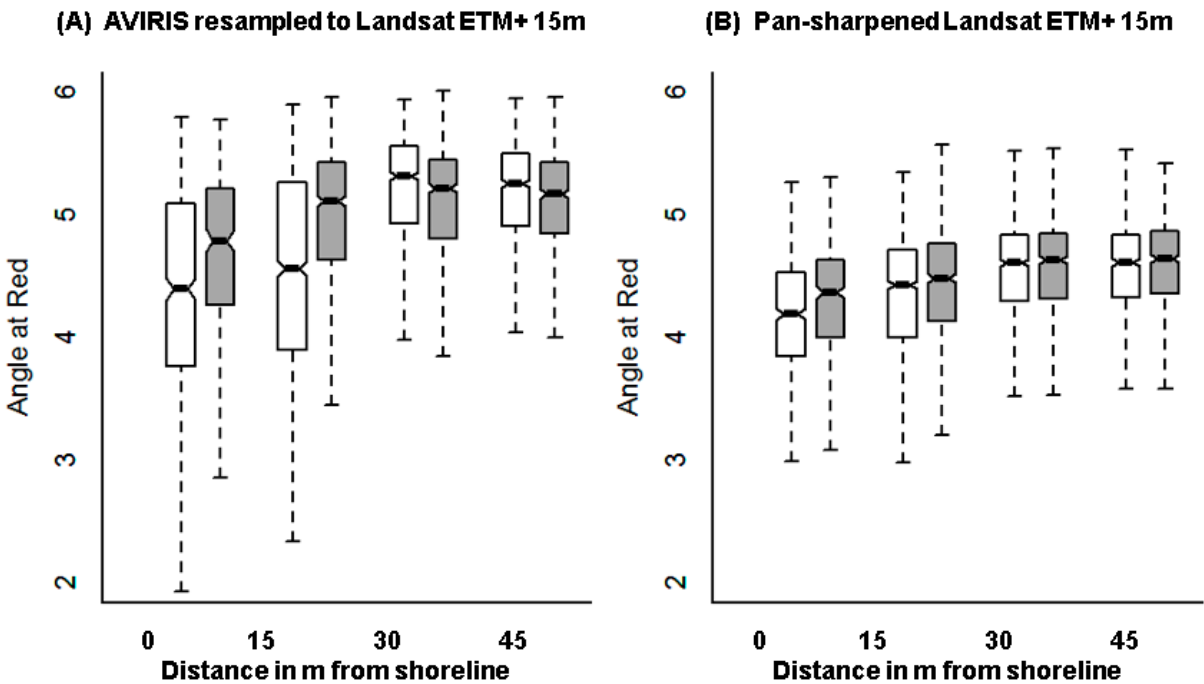gray.

Figure 7. Angle at Red vs. distance from shoreline in meters for (*a*) AVIRIS resampled to Landsat 15m and (*b*) actual Landsat ETM+ 15m pan-sharpened imagery. Distribution of the index along the oiled shoreline is in white and along oil-free shoreline is in gray.

Landsat comparisons using NDII also showed that AVIRIS$_{LS-15m}$ imagery produced higher effect sizes than the pan-sharpened Landsat ETM+ 15m imagery (Table 6). For the Landsat 30m image, we found no significant differences among oiled and oil-free shores while the AVIRIS$_{LS-30m}$ was still able to differentiate oiled conditions for the first 30m inland (1 pixel).

363   **Table 6.** Student t-test comparison results for NDII calculated from AVIRIS imagery spectrally and spatially
364   resampled to Landsat (AVIRIS$_{LS}$) 15m and 30m compared to the actual Landsat imagery. Bold p-values are
365   significant at the 0.05 level. Value of Cohen's d indicates effect size.

Sensor	Zone	N		Means		Std. Dev.		Student t-Statistic	p-value	Cohen's d
		oiled	oil-free	oiled	oil-free	oiled	oil-free			
AVIRIS$_{LS}$ 15m	1	1318	852	0.431	0.540	0.172	0.130	16.772	**0.000**	0.695
Landsat 15m	1	596	392	0.221	0.252	0.060	0.047	-9.279	**0.000**	0.573
AVIRIS$_{LS}$ 30m	1	749	405	0.498	0.553	0.120	0.100	-8.359	**0.000**	0.489
Landsat 30m	1	467	98	0.254	0.397	0.422	0.907	-1.517	0.132	*

* Cohen's d not reported for Landsat ETM+ 30m image because the p-value is not significant.

366

4   Discussion

368   Selecting the appropriate remote sensing data to detect and monitor impacts of oil spills and

369   recovery involves a careful consideration of cost and ability to achieve goals as no single sensor

370   meets all the requirements needed for achieving such a task. Here, we set out to assess whether

371   sensor spatial and spectral resolution, and sensor characteristics influence the ability to detect

372   and map vegetation stress and die-off due to oil spills.

4.1 Spectral resolution

374   AVIRIS$_{WV2}$ has the same spatial resolution as AVIRIS in this study (3.5m) but broad-bands of

375   40-180nm width instead of the 10nm narrow-bands of the AVIRIS sensor. Thus, the effect

376   spectral resolution is examined by comparing their performance. Several studies have shown that

377   fine spectral resolution is important for species-level classification [22,92-94], in some cases,

378   even more important than spatial resolution [95,96]. However, when the goal is to detect plant

379   stress, especially when using indices, coarser spectral resolution may be sufficient, particularly

380   when combined with fine spatial resolution [97,98]. Teillet et al. [97] calculated NDVI at various

381   spatial and spectral resolutions and found that when bandwidth of the Red band increased

382   beyond 50 nm, there was an appreciable drop in the ability of the index to track plant health, and

383   found similar results for other indices. As the Red band width for all three multispectral sensors

384   we used is greater than 50 nm, this is consistent with the above reported decrease in ability to

385   track plant health (Red bandwidth, RapidEye: 55nm, WorldView2: 60nm, and Landsat ETM+:

386   60nm). Hence, it is expected that the loss of spectral resolution will degrade the ability to

387   discriminate oil-induced plant stress. Our study demonstrated that there was loss of ability to

388   detect vegetation stress with broader spectral bands, as AVIRIS was able to detect significant

389   differences in vegetation index values up to 14m inland (inland zones with lower oil impact) but

390   $AVIRIS_{WV2}$ could not. Additionally, index value differences were weaker when using

391   $AVIRIS_{WV2}$ in all zones.

392   Multiple studies have also pointed out the importance of a wider spectral range, specifically the

393   advantage of having SWIR bands for detecting vegetation and vegetation stress [99-101]. Of the

394   three multispectral sensors we tested, only Landsat ETM+ has SWIR bands, which we used to

395   calculate NDII. The results of the Landsat NDII comparison showed that for $AVIRIS_{LS-15m}$,

396   $AVIRIS_{LS-30m}$ and LS-15m there was a stronger differentiation between oiled and oil-free

397   shorelines using NDII than using ARed (no SWIR band). However, with the LS-30m sensor

398   data, ARed detected a significant response while NDII did not, indicating that this wider spectral

399   range is not always necessary, which is likely due to an interaction with the effect of spatial

400   resolution. However, such interactions between wider spectral range and spatial resolution need

401   further investigation. Furthermore, a comparison of ARed and NDII using AVIRIS 3.5m narrow-

402   band data showed that ARed performed as well as NDII, again indicating that the presence of the

403   SWIR band might not be critical to detection of vegetation stress. This could be because

404   vegetation stress is identifiable across multiple regions of the electro-magnetic spectrum [37].

405   *4.2 Spatial resolution*

406   The choice of the appropriate spatial resolution is important for the detection of oil-induced

407   vegetation stress, and critical for the precise identification of the boundaries of the affected area.

408   In this particular study, the impact was localized to a narrow 14m band along the affected

409   shoreline [20], and the degree of impact differed with distance from the shore. Hence it was

410   important to have a spatial resolution finer than 14m to delineate this oil impact. These impacts

411   were easily detected at all resolutions except at Landsat 30m, but effect sizes declined rapidly as

412   spatial resolution became coarser. At the Landsat 30m pixel resolution, half of the area within

413   the first pixel next to the shore is not affected by oil and the impacted vegetation is intermixed

414   with healthy vegetation. This reduces the effect size, making it difficult to detect significant

415   differences between stressed and non-stressed vegetation. However, to detect the gradient of

416   stress inland from the shoreline, and to delineate the affected area with some degree of

417   confidence, a finer spatial resolution is required as demonstrated by our results. Studies by

418   Teillet et al. [97] and Paul et al. [102] suggested that required spatial resolution depends on the

419   study goals and that coarse spatial resolution was sufficient for studies involving large targets.

420   For example, Paul et al. [102] were trying to map the extent of debris-free glaciers wider than

421   100m and found the Landsat TM resolution of 30m to be sufficient. The results of our study

422   corroborate this assertion that the aims of the study determine the resolution required. In this

423   study, Landsat pan-sharpened 15 m imagery would have been sufficient to determine the length

424   of shoreline affected by the oil spill, but would not be able to identify the depth of penetration or

425   delineate the affected area. By using finer spatial resolution sensors like AVIRIS or

426   WorldView2, we were able to examine depth and magnitude of oil impacts on vegetation. Our

427   study site, Barataria Bay, has a consistent topography where a gradual increase in elevation at the

428   shore creates distinct subtidal, intertidal and upland areas. The oil, coming in from offshore,

429   penetrated to the high-tide mark thus confining the impact of the spill in a narrow 14m band by

430   the shoreline [20]. However, in other regions in the gulf, a different hydrology and topography

431   forced a different outcome from the DWH oil spill [103]. For example, in low-lying Chandeleur

432   island mangroves, the tide penetrated much further spreading oil more uniformly and likely

433   causing mortality due to coating of pneumatophores rather than the mangrove canopy and leaves

434   [103]. Thus, in the mangrove ecosystem, coarser resolution imagery might have proved

435   sufficient for identifying the impacted coastline as well as the area affected.

436   *4.3 Sensor signal-to-noise ratio (SNR)*

437   While all multispectral sensors were successful in detecting significant vegetation stress along

438   the oiled shores relative to oil-free shores, their performance was consistently inferior to

439   AVIRIS. This remained true even when AVIRIS was spectrally and spatially resampled to match

440   these other sensors. This suggests that factors other than spectral and spatial resolution also play

441   a role in the performance.

442   The radiometric resolution of the four sensors tested in this study ranged from 8-bit quantization

443   in Landsat images to 16-bit quantization for AVIRIS and RapidEye (Table 1). Since oil darkens

444   the albedo in most bands from the visible to the SWIR, the radiometric *range* is unlikely to have

445   a large impact on performance. Moreover, RapidEye performed no better than WorldView2

446   despite having higher radiometric *resolution*, suggesting that radiometric resolution did not affect

447   performance. However, RapidEye has coarser spatial resolution compared to WorldView2 hence

448   it is not possible to completely isolate the effect of radiometric resolution from the effect of

449   spatial scale. Therefore, more specific tests might be needed to examine how radiometric

450   resolution affects performance.

451   The signal-to-noise ratio of AVIRIS in both the visible and NIR regions is better than any of the

452   other sensors [71-75]. Additionally, when AVIRIS was resampled to the multispectral sensors'

453   characteristics, it likely performed better because each new band was calculated from the sum of

454   several narrow bands with high SNR, increasing the signal strength of the resampled image [71].

455   Better SNR implies that the sensor is more likely to detect vegetation stress when present, and

456   also more likely to discriminate small differences in vegetation stress. There are very few studies

457   that compare the performance of different sensors based on their SNR. Platt and Goetz [71]

458   compared AVIRIS performance to Landsat and concluded that the advantage of AVIRIS over

459   Landsat when classifying land cover was due to spectral resolution, not SNR. However, the

460   current study suggests that the AVIRIS signal is stronger compared to that of the other sensors,

461   even when spectrally resampled.

462   Factors other than SNR may also have influenced the performance of the multispectral sensors.

463   Both WorldView2 and RapidEye images were acquired off-nadir at oblique angles which can

464   increase scattering across pixels, therefore making it more difficult to separate oiled from non-

465   oiled areas. Additionally, multispectral sensors lack the narrow bands that allow accurate

466   estimates of water vapor in the atmosphere and help achieve a better atmospheric calibration.

467   Current (e.g., Landsat 8, WorldView3, Sentinel-2) and future sensors may have SNR comparable

468   to AVIRIS. A comparison with these sensors might yield different results. Landsat 8 was

469   launched in 2013, WorldView3 in 2014, and Sentinel-2 in 2015, hence they were unavailable at

470   the time of this oil spill in 2010, but could be useful for future disasters.

471   *4.4 Timing of image acquisition*

472   The WorldView2 imagery, while successful in detecting oil impacts, indicated a narrower

473   shoreline zone affected by oil compared to the AVIRIS imagery. This is likely because the

474   WorldView2 data were acquired at high tide. Tide levels were 29cm higher at the time the

475   WorldView2 images were acquired, compared to the AVIRIS image (NOAA,

476   http://tidesandcurrents.noaa.gov/). This highlights the importance of tidal effects when the study

477   area is dynamic and water levels are changing throughout the day. It is important to schedule

478   image acquisitions (where possible e.g., in the case of airborne imagery) at low tide to expose

479   maximum possible land area. In our study, this was especially important because the oil came

480   inland from the shoreline resulting in the most affected area being next to the shore. In addition,

481   this could also explain the poor performance of Rapid Eye, which was collected almost a month

482   later than the data from the other sensors. With satellite imagery, there is very little control over

483   the time of acquisition which can result in underestimation of the affected area and its impacts on

484   vegetation stress.

5   Conclusion

486   Multispectral sensor imagery is relatively more economical than hyperspectral imagery and is

487   now often available at a fine spatial resolution making it an excellent tool for mapping impact

488   and monitoring recovery of ecosystems after environmental disasters such as oil spills, floods,

489   and hurricanes. This study examined the potential of three multispectral sensors with

490   considerably less financial costs than AVIRIS (i.e., WorldView2 is estimated at half the cost of

491   AVIRIS, RapidEye at a fraction of the cost, and Landsat ETM+ is free) for mapping the extent of

492   the impact of the 2010 DWH oil spill on the wetlands of Louisiana. However, if accuracy is

493   prioritized, clearly AVIRIS data performed the best, even when resampled to coarser spectral

494   and spatial resolutions. This indicates that sensor characteristics, such as signal-to-noise ratio, are

495   critical in detecting vegetation stress. WorldView2 and RapidEye were unable to detect oil

496   impact to the same inland distance as AVIRIS. In the case of WorldView2 this might be because

497   of high tides covering oiled areas denuded of vegetation, and in the case of RapidEye the late

498   acquisition date. Landsat ETM+ 15m data gave mixed results likely due to its coarse spatial

499   resolution.

500   Spatial resolution was therefore the most critical factor limiting the detection of the extent of oil

501   impact although spectral resolution and sensor characteristics (e.g. SNR, sensor view angle, etc.)

502   also limited the ability to detect vegetation stress. Based on these results we suggest that since no

503   sensor has all of the characteristics necessary to detect extent, impact, and recovery from oil

504   spills, it is important to determine which sensor is best for the objectives of a particular project.

505   If the objective is to map the extent of oil impact, sensors like WorldView2 and RapidEye, or

506   even Landsat, are sufficient if the impact is widespread. If the objective is to detect vegetation

507   stress and recovery, and delineate the affected area for treatment, then it is important to have

508   high spectral and spatial resolution collected at the optimal time to reveal the stress, as these

509   characteristics allow for detecting even subtle differences in vegetation condition. The results of

510   this study provide important guidelines for sensor selection which requires careful consideration

511   of the extent of impact, location of the affected area, degree of complexity required in detection

512   of impact, and characteristics of the study area which might require specific timing of image

513   acquisition.

514   **Acknowledgements**

Author Contributions

521   SK wrote the manuscript, conducted most of the analysis, and interpreted results. MJS provided

522   critical advice on analysis methods and interpretation of results and helped with every section of

523   the written manuscript. SLU provided lab resources, advice on methods and interpretation, and

524   edited the manuscript. KS, PJH and ML helped in preparing and preprocessing image data,

525   extracting data for analysis and editing the manuscript.

Conflict of Interest

527   The authors declare no conflict of interest.

References

529

530   1.   Reimold, R.J.; Hardisky, M.A. Nonconsumptive use of values of wetlands. In *Wetland functions*
531   *and values*, Greeson, P.E.; Clark, J.R.; Clark, J.E., Eds. American Water Resources Association:
532   Minneapolis, MN, 1979; pp 558-564.
533   2.   Barbier, E.B.; Hacker, S.D.; Kennedy, C.; Koch, E.W.; Stier, A.C.; Silliman, B.R. The value of
534   estuarine and coastal ecosystem services. *Ecol. Monogr.* **2011**, *81*, 169-193.
535   3.   Barbier, E.B.; Koch, E.W.; Silliman, B.R.; Hacker, S.D.; Wolanski, E.; Primavera, J.; Granek, E.F.;
536   Polasky, S.; Aswani, S.; Cramer, L.A.*, et al.* Coastal ecosystem-based management with nonlinear
537   ecological functions and values. *Sci* **2008**, *319*, 321-323.
538   4.   Kirwan, M.L.; Megonigal, J.P. Tidal wetland stability in the face of human impacts and sea-level
539   rise. *Nature* **2013**, *504*, 53-60.
540   5.   Liquete, C.; Piroddi, C.; Drakou, E.G.; Gurney, L.; Katsanevakis, S.; Charef, A.; Egoh, B. Current
541   status and future prospects for the assessment of marine and coastal ecosystem services: A
542   systematic review. *PLOS ONE* **2013**, *8*, e67737.

543 6.   Temmerman, S.; Meire, P.; Bouma, T.J.; Herman, P.M.J.; Ysebaert, T.; De Vriend, H.J. Ecosystem-
544   based coastal defence in the face of global change. *Nature* **2013**, *504*, 79-83.
545 7.   Duarte, C.M.; Losada, I.J.; Hendriks, I.E.; Mazarrasa, I.; Marba, N. The role of coastal plant
546   communities for climate change mitigation and adaptation. *Nature Clim. Change* **2013**, *3*, 961-
547   968.
548 8.   Möller, I.; Kudella, M.; Rupprecht, F.; Spencer, T.; Paul, M.; van Wesenbeeck, B.K.; Wolters, G.;
549   Jensen, K.; Bouma, T.J.; Miranda-Lange, M*., et al.* Wave attenuation over coastal salt marshes
550   under storm surge conditions. **2014**, *7*, 727.
551 9.   Blum, M.D.; Roberts, H.H. Drowning of the mississippi delta due to insufficient sediment supply
552   and global sea-level rise. *Nature Geoscience* **2009**, *2*, 488-491.
553 10. Blum, M.D.; Roberts, H.H. The mississippi delta region: Past, present, and future. *AREPS* **2012**,
554   *40*, 655-683.
555 11. Day, J.; Britsch, L.; Hawes, S.; Shaffer, G.; Reed, D.; Cahoon, D. Pattern and process of land loss in
556   the mississippi delta: A spatial and temporal analysis of wetland habitat change. *Estuaries* **2000**,
557   *23*, 425-438.
558 12. Conner, W.; Day, J., Jr.; Baumann, R.; Randall, J. Influence of hurricanes on coastal ecosystems
559   along the northern gulf of mexico. *Wetlands Ecol. Manage.* **1989**, *1*, 45-56.
560 13. Gundlach, E.R.; Hayes, M.O. Vulnerability of coastal environments to oil spill impacts. *Mar.*
561   *Technol. Soc. J.* **1978**, *12*, 18-27.
562 14. Burk, J.C. A four year analysis of vegetation following an oil spill in a freshwater marsh. *J. Appl.*
563   *Ecol.* **1977**, *14*, 515-522.
564 15. Hester, M.W.; Mendelssohn, I.A. Long-term recovery of a louisiana brackish marsh plant
565   community from oil-spill impact: Vegetation response and mitigating effects of marsh surface
566   elevation. *Mar. Environ. Res.* **2000**, *49*, 233-254.
567 16. Lin, Q.; Mendelssohn, I.A. Impacts and recovery of the deepwater horizon oil spill on vegetation
568   structure and function of coastal salt marshes in the northern gulf of mexico. *Environ. Sci.*
569   *Technol.* **2012**, *46*, 3737-3743.
570 17. Ramseur, J.L. *Oil spills in u.S. Coastal waters: Background, governance, and issues for congress*;
571   Congressional Research Service: 2010.
572 18. Moss, L. The 13 largest oil spills in history. In *Mother Nature Network*, Narrative Content Group:
573   Atlanta, Georgia, 2010.
574 19. Judy, C.R.; Graham, S.A.; Lin, Q.; Hou, A.; Mendelssohn, I.A. Impacts of macondo oil from
575   deepwater horizon spill on the growth response of the common reed phragmites australis: A
576   mesocosm study. *Mar. Pollut. Bull.* **2014**, *79*, 69-76.
577 20. Khanna, S.; Santos, M.J.; Ustin, D.S.L.; Koltunov, A.; Kokaly, R.F.; Roberts, D.A. Detection of salt
578   marsh vegetation stress after the deepwater horizon bp oil spill along the shoreline of gulf of
579   mexico using aviris data. *PloS ONE* **2013**, *8*, e78989.
580 21. Lin, Q.; Mendelssohn, I.A.; Graham, S.A.; Hou, A.; Fleeger, J.W.; Deis, D.R. Response of salt
581   marshes to oiling from the deepwater horizon spill: Implications for plant growth, soil surface-
582   erosion, and shoreline stability. *Sci. Total Environ.* **2016**, *557–558*, 369-377.
583 22. Mishra, D.R.; Cho, H.J.; Ghosh, S.; Fox, A.; Downs, C.; Merani, P.B.T.; Kirui, P.; Jackson, N.;
584   Mishra, S. Post-spill state of the marsh: Remote estimation of the ecological impact of the gulf of
585   mexico oil spill on louisiana salt marshes. *Remote Sens. Environ.* **2012**, *118*, 176-185.
586 23. Silliman, B.R.; van de Koppel, J.; McCoy, M.W.; Diller, J.; Kasozi, G.N.; Earl, K.; Adams, P.N.;
587   Zimmerman, A.R. Degradation and resilience in louisiana salt marshes after the bp–deepwater
588   horizon oil spill. *Proceedings of the National Academy of Sciences* **2012**, *109*, 11234-11239.
589 24. Wiens, J.A. Review of an ecosystem services approach to assessing the impacts of the
590   deepwater horizon oil spill in the gulf of mexico. *Fisheries* **2015**, *40*, 86-86.

591   25.   Ko, J.Y.; Day, J.W. A review of ecological impacts of oil and gas development on coastal
592   ecosystems in the mississippi delta. *Ocean Coast. Manage.* **2004**, *47*, 597-623.
593   26.   Pezeshki, S.R.; Hester, M.W.; Lin, Q.; Nyman, J.A. The effects of oil spill and clean-up on
594   dominant us gulf coast marsh macrophytes: A review. *Environ. Pollut.* **2000**, *108*, 129-139.
595   27.   Smith, C.J.; Delaune, R.D.; Patrick, W.H.; Fleeger, J.W. Impact of dispersed and undispersed oil
596   entering a gulf coast salt marsh. *Environ. Toxicol. Chem.* **1984**, *3*, 609-616.
597   28.   Pezeshki, S.R.; DeLaune, R.D. United states gulf of mexico coastal marsh vegetation responses
598   and sensitivities to oil spill: A review. *Environments* **2015**, *2*, 586-607.
599   29.   Lin, Q.; Mendelssohn, I.A. A comparative investigation of the effects of south louisiana crude oil
600   on the vegetation of fresh, brackish and salt marshes. *Mar. Pollut. Bull.* **1996**, *32*, 202-209.
601   30.   Kenworthy, W.J.; Durako, M.J.; Fatemy, S.M.R.; Valavi, H.; Thayer, G.W. Ecology of seagrasses in
602   northeastern saudi arabia one year after the gulf war oil spill. *Mar. Pollut. Bull.* **1993**, *27*, 213-
603   222.
604   31.   Khanna, S.; Santos, M.; Koltunov, A.; Shapiro, K.; Lay, M.; Ustin, S. Marsh loss due to cumulative
605   impacts of hurricane isaac and the deepwater horizon oil spill in louisiana. *Remote Sensing* **2017**,
606   *9*, 169.
607   32.   Jackson, J.B.C.; Cubit, J.D.; Keller, B.D.; Batista, V.; Burns, K.; Caffey, H.M.; Caldwell, R.L.; Garrity,
608   S.D.; Getter, C.D.; Gonzalez, C.*, et al.* Ecological effects of a major oil spill on panamanian coastal
609   marine communities. *Sci* **1989**, *243*, 37-44.
610   33.   Walker, D.A.; Webber, P.J.; Everett, K.R.; Brown, J. Effects of crude and diesel oil spills on plant
611   communities at prudhoe bay, alaska, and the derivation of oil spill sensitivity maps. *Arctic* **1978**,
612   *31*, 242-259.
613   34.   Houborg, R.; Soegaard, H.; Boegh, E. Combining vegetation index and model inversion methods
614   for the extraction of key vegetation biophysical parameters using terra and aqua modis
615   reflectance data. *Remote Sens. Environ.* **2007**, *106*, 39-58.
616   35.   Jurgens, C. The modified normalized difference vegetation index (mndvi) a new index to
617   determine frost damages in agriculture based on landsat tm data. *Int. J. Remote Sens.* **1997**, *18*,
618   3583-3594.
619   36.   Peñuelas, J.; Gamon, J.A.; Griffin, K.L.; Field, C.B. Assessing community type, plant biomass,
620   pigment composition, and photosynthetic efficiency of aquatic vegetation from spectral
621   reflectance. *Remote Sens. Environ.* **1993**, *46*, 110-118.
622   37.   Ustin, S.L.; Gitelson, A.A.; Jacquemoud, S.; Schaepman, M.; Asner, G.P.; Gamon, J.A.; Zarco-
623   Tejada, P. Retrieval of foliar information about plant pigment systems from high resolution
624   spectroscopy. *Remote Sens. Environ.* **2009**, *113*, S67-S77.
625   38.   Zarco-Tejada, P.J.; Rueda, C.A.; Ustin, S.L. Water content estimation in vegetation with modis
626   reflectance data and model inversion methods. *Remote Sens. Environ.* **2003**, *85*, 109-124.
627   39.   Gitelson, A.; Merzlyak, M.N. Spectral reflectance changes associated with autumn senescence of
628   *aesculus-hippocastanum* l. And *acer-platanoides* l. Leaves - spectral features and relation to
629   chlorophyll estimation. *J. Plant Physiol.* **1994**, *143*, 286-292.
630   40.   Gitelson, A.A.; Merzlyak, M.N. Remote estimation of chlorophyll content in higher plant leaves.
631   *Int. J. Remote Sens.* **1997**, *18*, 2691 - 2697.
632   41.   Fensholt, R.; Sandholt, I. Derivation of a shortwave infrared water stress index from modis near-
633   and shortwave infrared data in a semiarid environment. *Remote Sens. Environ.* **2003**, *87*, 111-
634   121.
635   42.   Gao, B.C. Ndwi--a normalized difference water index for remote sensing of vegetation liquid
636   water from space. *Remote Sens. Environ.* **1996**, *58*, 257-266.
637   43.   Hunt, E.R.; Rock, B.N. Detection of changes in leaf water content using near-infrared and middle-
638   infrared reflectances. *Remote Sens. Environ.* **1989**, *30*, 43-54.

639　44.　Khanna, S.; Palacios-Orueta, A.; Whiting, M.L.; Ustin, S.L.; Riano, D.; Litago, J. Development of
640　　　　angle indexes for soil moisture estimation, dry matter detection and land-cover discrimination.
641　　　　*Remote Sens. Environ.* **2007**, *109*, 154-165.
642　45.　Lillesand, T.M.; Kiefer, R.W.; Chipman, J.W. *Remote sensing and image interpretation*. John
643　　　　Wiley & Sons, Inc.: New York, 2004.
644　46.　Richardson, A.J.; Wiegand, C.L. Distinguishing vegetation from soil background information.
645　　　　*Photogramm. Eng. Remote Sensing* **1977**, *43*, 1541-1552.
646　47.　Tucker, C.J. Red and photographic infrared linear combinations for monitoring vegetation.
647　　　　*Remote Sens. Environ.* **1979**, *8*, 127-150.
648　48.　Palacios-Orueta, A.; Whiting, M.L.; Ustin, S.L.; Litago, J.; Garcia, M.; Khanna, S. In *Cotton*
649　　　　*phenology analysis with the new remote sensing spectral angle indexes as1 and as2*,
650　　　　International Conference on Agricultural Engineering, Crete, Greece, 23-25 June, 2008, 2008;
651　　　　Crete, Greece.
652　49.　Li, L.; Ustin, S.L.; Lay, M. Application of aviris data in detection of oil-induced vegetation stress
653　　　　and cover change at jornada, new mexico. *Remote Sens. Environ.* **2005**, *94*, 1-16.
654　50.　Boochs, F.; Kupfer, G.; Dockter, K.; Kühbauch, W. Shape of the red edge as vitality indicator for
655　　　　plants. *Int. J. Remote Sens.* **1990**, *11*, 1741-1753.
656　51.　Carter, G.A. Responses of leaf spectral reflectance to plant stress. *Am. J. Bot.* **1993**, *80*, 239-243.
657　52.　Bammel, B.H.; Birnie, R.W. *Spectral reflectance response of big sagebrush to hydrocarbon-*
658　　　　*induced stress in the bighorn basin, wyoming*. American Society for Photogrammetry and
659　　　　Remote Sensing: Bethesda, MD, ETATS-UNIS, 1994; Vol. 60.
660　53.　Al-Awadhi, J.M.; Omar, S.A.; Misak, R.F. Land degradation indicators in kuwait. *LDD* **2005**, *16*,
661　　　　163-176.
662　54.　Cross, A.M. Monitoring marine oil pollution using avhrr data : Observation of the coast of kuwait
663　　　　and saudi arabia during january 1991. *Int. J. Remote Sens.* **1992**, *13*, 781-788.
664　55.　Bianchi, R.; Cavalli, R.M.; Marino, C.M.; Pignatti, S.; Poscolieri, M. In *Use of airborne*
665　　　　*hyperspectral images to assess the spatial distribution of oil spilled during the trecate blow-out*
666　　　　*(northern italy)*, SPIE, 1995; pp 352-362.
667　56.　Salem, F.; Kafatos, M. Hyperspectral image analysis for oil spill mitigation. In *22nd Asian*
668　　　　*Conference on Remote Sensing*, CRISP, Ed. Singapore, 2001.
669　57.　Brekke, C.; Solberg, A.H.S. Oil spill detection by satellite remote sensing. *Remote Sens. Environ.*
670　　　　**2005**, *95*, 1-13.
671　58.　DiGiacomo, P.M.; Washburn, L.; Holt, B.; Jones, B.H. Coastal pollution hazards in southern
672　　　　california observed by sar imagery: Stormwater plumes, wastewater plumes, and natural
673　　　　hydrocarbon seeps. *Mar. Pollut. Bull.* **2004**, *49*, 1013-1024.
674　59.　Simecek-Beatty, D.; Clemente-Colón, P. Locating a sunken vessel using sar imagery: Detection of
675　　　　oil spilled from the ss jacob luckenbach. *Int. J. Remote Sens.* **2004**, *25*, 2233-2241.
676　60.　Rosso, P.H.; Pushnik, J.C.; Lay, M.; Ustin, S.L. Reflectance properties and physiological responses
677　　　　of salicornia virginica to heavy metal and petroleum contamination. *Environ. Pollut.* **2005**, *137*,
678　　　　241-252.
679　61.　Van Der Meer, F.; Van Dijk, P.; Van Der Werff, H.; Yang, H. Remote sensing and petroleum
680　　　　seepage: A review and case study. *Terra Nova* **2002**, *14*, 1-17.
681　62.　Yang, H.; Zhang, J.; Van der Meer, F.; Kroonenberg, S.B. Geochemistry and field spectrometry for
682　　　　detecting hydrocarbon microseepage. *Terra Nova* **1998**, *10*, 231-235.
683　63.　Wilson, C.A.; Allison, M.A. An equilibrium profile model for retreating marsh shorelines in
684　　　　southeast louisiana. *Estuar. Coast. Shelf Sci.* **2008**, *80*, 483-494.
685　64.　Gosselink, J.G.; Pendleton, E.C. *The ecology of delta marshes of coastal louisiana: A community*
686　　　　*profile*; U. S. Fish and Wildlife Service: Washington DC, 1984; p 156.

687 65. Jones, C.E.; Minchew, B.; Holt, B.; Hensley, S. Studies of the *deepwater horizon* oil spill with the
688   uavsar radar. In *Monitoring and modeling the deepwater horizon oil spill: A record-breaking*
689   *enterprise*, AGU: Washington, DC, 2011; Vol. 195, pp 33-50.
690 66. Liu, P.; Li, X.; Qu, J.J.; Wang, W.; Zhao, C.; Pichel, W. Oil spill detection with fully polarimetric
691   uavsar data. *Mar. Pollut. Bull.* **2011**, *62*, 2611-2618.
692 67. Michel, J.; Owens, E.H.; Zengel, S.; Graham, A.; Nixon, Z.; Allard, T.; Holton, W.; Reimer, P.D.;
693   Lamarche, A.; White, M.*, et al.* Extent and degree of shoreline oiling: *Deepwater horizon* oil spill,
694   gulf of mexico, USA. *PLoS ONE* **2013**, *8*, e65087.
695 68. Ramsey III, E.; Rangoonwala, A.; Suzuoki, Y.; Jones, C.E. Oil detection in a coastal marsh with
696   polarimetric synthetic aperture radar (sar). *Remote Sensing* **2011**, *3*, 2630-2662.
697 69. Kokaly, R.F.; Couvillion, B.R.; Holloway, J.M.; Roberts, D.A.; Ustin, S.L.; Peterson, S.H.; Khanna, S.;
698   Piazza, S.C. Spectroscopic remote sensing of the distribution and persistence of oil from the
699   deepwater horizon spill in barataria bay marshes. *Remote Sens. Environ.* **2013**, *129*, 210-230.
700 70. Kokaly, R.F.; Heckman, D.; Holloway, J.; Piazza, S.C.; Couvillion, B.R.; Steyer, G.D.; Mills, C.T.;
701   Hoefen, T.M. *Shoreline surveys of oil-impacted marsh in southern louisiana, july to august 2010*;
702   2011.
703 71. Platt, R.V.; Goetz, A.F.H. A comparison of aviris and landsat for land use classification at the
704   urban fringe. *Photogrammetric Engineering & Remote Sensing* **2004**, *70*, 813-819.
705 72. Miecznik, G.; Grabowska, D. In *Worldview-2 bathymetric capabilities*, Algorithms and
706   Technologies for Multispectral, Hyperspectral, and Ultraspectral Imagery XVIII, Baltimore,
707   Maryland, USA, 2012; Baltimore, Maryland, USA, pp 83901J-83901J-83910.
708 73. Brunn, A.; Freedman, E.; Fleming, R. New resampling kernel and its effect on rapideye imagery.
709   http://www.serioussciencellc.com/files/CMTF_JACIE2013.pdf (9/2/2014),
710 74. Reulke, R.; Weichelt, H. Snr evaluation of the rapideye space-borne cameras. *Photogrammetrie -*
711   *Fernerkundung - Geoinformation* **2012**, *2012*, 29-38.
712 75. Mika, A.M. Three decades of landsat instruments. *Photogrammetric Engineering & Remote*
713   *Sensing* **1997**, *63*, 839-852.
714 76. Richter, R.; Schläpfer, D. Geo-atmospheric processing of airborne imaging spectrometry data.
715   Part 2: Atmospheric/topographic correction. *Int. J. Remote Sens.* **2002**, *23*, 2631-2649.
716 77. Ben-Dor, E.; Kindel, B.C.; Patkin, K. In *A comparison between six model-based methods to*
717   *retrieve surface reflectance and water vapor content from hyperspectral data: A case study using*
718   *synthetic aviris data*, International Conference on Optoelectronics, Dehradun, India, 2005;
719   Dehradun, India.
720 78. Koltunov, A.; Ben-Dor, E.; Ustin, S.L. Image construction using multitemporal observations and
721   dynamic detection models. *Int. J. Remote Sens.* **2008**, *30*, 57-83.
722 79. Koltunov, A.; Ustin, S.L.; Quayle, B.; Schwind, B. Goes early fire detection (goes-efd) system
723   prototype. In *ASPRS 2012 Anuual Conference*, Sacramento, CA, 2012.
724 80. Khanna, S.; Santos, M.J.; Ustin, S.L.; Haverkamp, P.J. An integrated approach to a
725   biophysiologically based classification of floating aquatic macrophytes. *Int. J. Remote Sens.* **2011**,
726   *32*, 1067-1094.
727 81. Clark, R.N.; Roush, T.L. Reflectance spectroscopy - quantitative analysis techniques for remote
728   sensing applications. *JGR* **1984**, *89*, 6329-6340.
729 82. Kokaly, R.F.; Heckman, D.; Holloway, J.; Piazza, S.; Couvillion, B.; Steyer, G.D.; Mills, C.; Hoefen,
730   T.M. *Shoreline surveys of oil-impacted marsh in southern louisiana, july to august 2010*; U.S.
731   Geological Survey: 2011; p 124.
732 83. Rosenfield, G.H.; Fitzpatrick-Lins, K. A coefficient of agreement as a measure of thematic
733   classification accuracy. *Photogramm. Eng. Remote Sensing* **1986**, *52*, 223-227.

734   84.   Story, M.; Congalton, R.G. Accuracy assessment - a user's perspective (map interpretation).
735   *Photogramm. Eng. Remote Sensing* **1986**, *52*, 397-399.
736   85.   Laben, C.A.; Brower, B.V. Process for enhancing the spatial resolution of multispectral imagery
737   using pan-sharpening. Google Patents: 2000.
738   86.   Mitsch, W.J.; Gosselink, J.G. *Wetlands*. John Wiley & Sons, Inc: New York, NY, USA, 2007.
739   87.   Hardisky, M.A.; Klemas, V.; Smart, R.M. The influence of soil-salinity, growth form, and leaf
740   moisture on the spectral radiance of *spartina-alterniflora* canopies. *Photogramm. Eng. Remote*
741   *Sensing* **1983**, *49*, 77-83.
742   88.   Palacios-Orueta, A.; Khanna, S.; Litago, J.; Whiting, M.L.; Ustin, S.L. In *Assessment of ndvi and*
743   *ndwi spectral indices using modis time series analysis and development of a new spectral index*
744   *based on modis shortwave infrared bands*, 1st international conference of remote sensing and
745   geoinformation processing, Trier, Germany, September 7-9, 2005; Trier, Germany, p 207–209.
746   89.   Cohen, J. *Statistical power analysis for the behavioral sciences*. Academic Press: New York, 1969.
747   90.   Cohen, J. *Statistical power analysis for the behavioral sciences*. Second ed.; Lawrence Earlbaum
748   Associates: Hillsdale, NJ, 1988.
749   91.   Khanna, S.; Santos, M.J.; Hestir, E.L.; Ustin, S.L. Plant community dynamics relative to the
750   changing distribution of a highly invasive species, *eichhornia crassipes*: A remote sensing
751   perspective. *Biol. Invasions* **2012**, *14*, 717-733.
752   92.   Cho, H.; Lee, K.-S. Comparison between hyperspectral and multispectral images for the
753   classification of coniferous species. *Korean Journal of Remote Sensing* **2014**, *30*, 25-36.
754   93.   Govender, M.; Chetty, K.; Naiken, V.; Bulcock, H. A comparison of satellite hyperspectral and
755   multispectral remote sensing imagery for improved classification and mapping of vegetation.
756   2008; Vol. 34, pp 147-154.
757   94.   Santos, M.J.; Hestir, E.L.; Khanna, S.; Ustin, S.L. Image spectroscopy and stable isotopes elucidate
758   functional dissimilarity between native and nonnative plant species in the aquatic environment.
759   *New Phytol.* **2012**, *193*, 683-695.
760   95.   Mumby, P.J.; Edwards, A.J. Mapping marine environments with ikonos imagery: Enhanced
761   spatial resolution can deliver greater thematic accuracy. *Remote Sens. Environ.* **2002**, *82*, 248-
762   257.
763   96.   Underwood, E.; Ustin, S.; Ramirez, C. A comparison of spatial and spectral image resolution for
764   mapping invasive plants in coastal california. *Environ. Manage.* **2007**, *39*, 63-83.
765   97.   Teillet, P.M.; Staenz, K.; William, D.J. Effects of spectral, spatial, and radiometric characteristics
766   on remote sensing vegetation indices of forested regions. *Remote Sens. Environ.* **1997**, *61*, 139-
767   149.
768   98.   van Wagtendonk, J.W.; Root, R.R.; Key, C.H. Comparison of aviris and landsat etm+ detection
769   capabilities for burn severity. *Remote Sens. Environ.* **2004**, *92*, 397-408.
770   99.   Asner, G.P.; Heidebrecht, K.B. Spectral unmixing of vegetation, soil and dry carbon cover in arid
771   regions: Comparing multispectral and hyperspectral observations. *Int. J. Remote Sens.* **2002**, *23*,
772   3939-3958.
773   100. Bach, H.; Mauser, W. In *Improvements of plant parameter estimations with hyperspectral data*
774   *compared to multispectral data*, Remote Sensing of Vegetation and Sea, Taormina, Italy, 1997;
775   SPIE: Taormina, Italy, pp 59-67.
776   101. Lee, K.-S.; Cohen, W.B.; Kennedy, R.E.; Maiersperger, T.K.; Gower, S.T. Hyperspectral versus
777   multispectral data for estimating leaf area index in four different biomes. *Remote Sens. Environ.*
778   **2004**, *91*, 508-520.
779   102. Paul, F.; Huggel, C.; Kääb, A.; Kellenberger, T.; Maisch, M. In *Comparison of tm-derived glacier*
780   *areas with higher resolution data sets*, EARSeL - LISSIG - Workshop Observing our Cryosphere
781   from Space, Bern, Switzerland, March 11-13, 2002; Bern, Switzerland.

103. Shapiro, K.; Khanna, S.; Ustin, S.L. In *Differential impact and recovery of oil-induced stress on three diverse sites in the gulf of mexico due to the bp deepwater horizon oil spill*, Ecological Society of America, Sacramento, California, USA, August 10-14, 2014, 2014; Sacramento, California, USA.

Figure Captions

Figure 1: AVIRIS gray scale image of Barataria Bay and its location in the Mississippi Delta. Oil mapped using AVIRIS 2010 imagery is overlaid in red.

Figure 2: Barataria Bay gray scale image subset for all four sensors and a close view of a smaller region to highlight differences in image quality and spatial resolution (a) AVIRIS 3.5m imagery, (b) WorldView2 2m imagery, (c) RapidEye 5m imagery, and (d) Landsat ETM+ 30m imagery.

Figure 3: An example of (a) green vegetation and (b) non-photosynthetic vegetation (NPV) pixel spectra from AVIRIS, WorldView2, RapidEye, and Landsat ETM+ showing the range and spectral resolution of the sensors.

Figure 4. Boxplots of the Angle at Red index in the first pixel zone along oiled (white) vs. oil-free (gray) shoreline using AVIRIS imagery resampled to WorldView2, Landsat ETM+ 15m and Landsat ETM+ 30m. Notches on the boxplots indicate the 95% confidence interval. Cohen's d values are shown for reference at the top.

Figure 5. A subset of Barataria Bay shown in gray scale (*a*) AVIRIS, (*b*) WorldView-2, (*c*) RapidEye, (*d*) Landsat ETM+ pan sharpened 15m, (*e*) Landsat ETM+ 30m with oiled pixels overlaid in red. NDVI color map of an oiled and an oil-free area is detailed in the second and third rows from the top. Note the lack of spatial definition of the affected area as spatial resolution deteriorates.

Figure 6. Angle at Red vs. distance from shoreline in meters for (*a*) AVIRIS resampled to RapidEye and (*b*) actual RapidEye imagery. Distribution of the index along the oiled shoreline is in white and along oil-free shoreline, in gray.

Figure 7. Angle at Red vs. distance from shoreline in meters for (*a*) AVIRIS resampled to Landsat 15m and (*b*) actual Landsat ETM+ 15m pan-sharpened imagery. Distribution of the index along the oiled shoreline is in white and along oil-free shoreline is in gray.

Table Captions

810

811

812   **Table 1:** Characteristics of the four sensors and date of image acquisition for data analyzed in this study.

813   **Table 2:** Vegetation indices used to test for the effects of oil contamination on vegetation stress, and the sensors
814   they were calculated for. R_G, R_R, R_{NIR} and R_{SWIR} are the reflectance values in the Green (G), Red (R), Near InfraRed
815   (NIR) and ShortWave InfraRed (SWIR) bands respectively and λ_G (550-570nm), λ_R (650nm), λ_{NIR} (805-840nm) and
816   λ_{SWIR} (1650nm) are the wavelength values at the band centers.

817   **Table 3:** Student t-test comparison results for four indices calculated with AVIRIS data. Value of Cohen's d
818   indicates effect size.

819   **Table 4:** Student t-test comparison results for **ARed** in radians calculated from AVIRIS narrow-band image and
820   AVIRIS imagery spectrally and spatially resampling to WorldView2 (AVIRIS$_{WV2}$), RapidEye (AVIRIS$_{RE}$), and
821   Landsat (AVIRIS$_{LS}$) 15m and 30m. Value of Cohen's d indicates effect size.

822   **Table 5.** Student t-test comparison results for **ARed** in radians calculated from AVIRIS imagery spectrally and
823   spatially resampled to WorldView2 (AVIRIS$_{WV2}$), RapidEye (AVIRIS$_{RE}$), Landsat (AVIRIS$_{LS}$) 15m and 30m
824   compared to the actual sensor imagery. Value of Cohen's d indicates effect size.

825   **Table 6.** Student t-test comparison results for NDII calculated from AVIRIS imagery spectrally and spatially
826   resampled to Landsat (AVIRIS$_{LS}$) 15m and 30m compared to the actual Landsat imagery. Bold p-values are
827   significant at the 0.05 level. Value of Cohen's d indicates effect size.

828